

Article

A Flexible Meta-Curtain for Simultaneous Soundproofing and Ventilation

Xiaobin Cui ¹, Chenkai Liu ^{2,*} , Jinjie Shi ², Changhui Shen ², Xiaozhou Liu ^{2,*}  and Yun Lai ^{2,*} ¹ School of Physical and Mathematical Sciences, Nanjing Tech University, Nanjing 211816, China² MOE Key Laboratory of Modern Acoustics, National Laboratory of Solid State Microstructures, School of Physics, Collaborative Innovation Center of Advanced Microstructures, Nanjing University, Nanjing 210093, China

* Correspondence: liuck@nju.edu.cn (C.L.); xzliu@nju.edu.cn (X.L.); laiyun@nju.edu.cn (Y.L.)

Abstract: We demonstrate a flexible meta-curtain that can simultaneously block the propagation of sound waves of selected frequencies and let air flow through freely. Such a meta-curtain is assembled by two soft and perforated polyvinyl chloride films with an optimized distance between them. The total thickness of the meta-curtain is 1.16 cm and the holes on it have a diameter of 5 cm. The functionality of soundproofing is bestowed by the resonances formed between the films, which is verified by band structure analysis, numerical simulations, and experimental measurements. We experimentally observed sound transmission loss with a peak of 50 dB near 1700 Hz and an average of 26 dB from 1000 Hz to 1760 Hz, which is consistent with the numerical results. Attributing to the softness of the films and the robustness of the resonance, this meta-curtain retains its functionality even at deformations such as bending. Our work paves a way toward soundproof structures with the advantages of ventilation, flexibility, and light weight.

Keywords: acoustic metamaterial; soundproof ventilation; flexibility

Citation: Cui, X.; Liu, C.; Shi, J.; Shen, C.; Liu, X.; Lai, Y. A Flexible Meta-Curtain for Simultaneous Soundproofing and Ventilation. *Symmetry* **2022**, *14*, 2348. <https://doi.org/10.3390/sym14112348>

Academic Editors: Guobiao Hu, Jasim Uddin, Junrui Liang and Junlei Wang

Received: 18 October 2022

Accepted: 4 November 2022

Published: 8 November 2022

Publisher's Note: MDPI stays neutral with regard to jurisdictional claims in published maps and institutional affiliations.



Copyright: © 2022 by the authors. Licensee MDPI, Basel, Switzerland. This article is an open access article distributed under the terms and conditions of the Creative Commons Attribution (CC BY) license (<https://creativecommons.org/licenses/by/4.0/>).

1. Introduction

There is a great demand in blocking noise while simultaneously allowing airflow in industry engineering and daily life. Therefore, artificial acoustic structures that simultaneously exhibit the functionalities of soundproofing and ventilation have attracted an increasing amount of attention in recent decades [1]. Recently, acoustic artificial microstructures, namely acoustic metamaterials [2] and metasurfaces [3], offer unprecedented ways to manipulate sound waves and enable wide applications such as acoustic stealth [4–6], topological acoustics [7–9], and super absorption [10], etc. By utilizing the physical mechanisms of local resonances [11–31], destructive interferences [32–41], or gradient-phase manipulations [42–44], a new class of meta-structures with a sub-wavelength thickness have been demonstrated to insulate or dissipate the low-frequency noise, meanwhile keeping airflow through them for the purpose of ventilation [45–47]. However, most of the previous designs were fabricated with rigid materials. This is because rigid structures can provide the hard boundaries necessary for the formation of strongly localized resonances. When the structure becomes softer and lighter, the hard boundaries are no longer valid and the original resonances could disappear. Nevertheless, rigid structures lack the flexibility and deformability that are desired in many scenarios. To the best of our knowledge, to date there has been no report to combine the designs for soundproofing and ventilation with the properties of flexibility and deformability.

Here, we demonstrate a flexible meta-curtain that exhibit the functionalities of soundproofing and ventilation. Unlike previous designs, this meta-curtain is composed of two soft and perforated PVC (polyvinyl chloride) thin films (thickness of 0.8 mm) separated by 1 cm, thus it is soft and flexible. Tiny small pillars are applied between the films to maintain the distance. As a result of the acoustic cavity formed between the films and

the antisymmetric modes therein as deaf bands, a large STL (sound transmission loss) over a broad bandwidth is clearly observed in both simulations and experiments. Since there are holes of a diameter of 5 cm on the meta-curtain, ventilation for fresh air and heat dissipation is allowed. The robust soundproofing performance of the meta-curtain under small deformation like bending has been verified experimentally. These results have confirmed the realization of practical soundproof ventilation structures based on soft and flexible materials like PVC films.

2. Design of Flexible Meta-Curtain

2.1. Geometry Design

Figure 1 provides the schematic diagram of the designed meta-curtain. Such a meta-curtain is simply splitting a thick perforated PVC film into two parallel layers of thin PVC films with an optimized distance between them, as shown in Figure 1a. Different from the hard-solid structures used in the previous works, the PVC material used in our design is soft, thus significantly increasing the flexibility in varying the shape of the meta-curtain. Circular holes are distributed in a square lattice with a lattice constant of l on the films for ventilation. The enlarged view of a curved unit cell is shown in Figure 1b. The unit cell of the films has a central circular hole with a diameter of D . An acoustic cavity with a height h is formed between the films, which is also the distance between the films. The thickness of the film is t . A parameter of averaged curvature, i.e., $\bar{K} = |\alpha/s|$, is used to describe the degree of deformation, where α is the rotation angle of the tangent and s is arc length. It is noteworthy that such structure can support acoustic local resonances, e.g., Helmholtz-like resonances [48], which can lead to the phenomenon of sound insulation. In order to keep the height h to be almost a constant upon small deformation of the meta-curtain, tiny small pillars are pasted inside the films at the corners of the unit cells. Soft rubber strips are used as the frame of the meta-curtain. Therefore, the acoustic cavity remains relatively robust even when the meta-curtain is bent or deformed, as has been verified by experiments later. The final weight of the meta-curtain is almost the same as the thick PVC film, because the pillars and the strips are tiny and their weight is negligible.

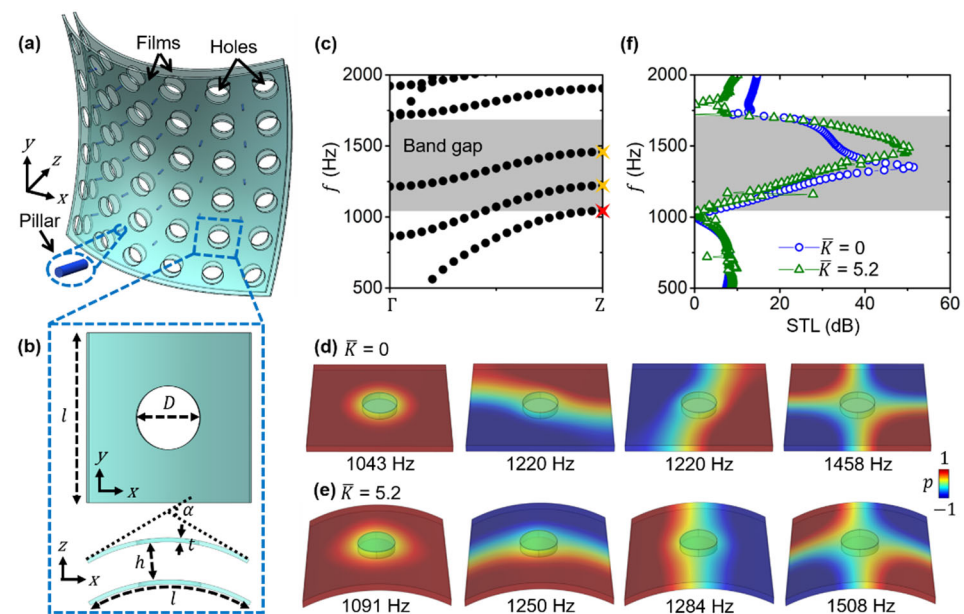


Figure 1. (a) Schematic diagram of the flexible meta-curtain, which is composed of two cascaded films separated by a certain distance. Circular holes are periodically distributed on the films for ventilation. (b) Front and side views of a curved unit cell. (c) Band structure of the meta-curtain with a flat shape. Eigenstates at the Z point (marked by red and orange stars in (c)) for (d) the flat unit cell and (e) the curved unit cell. (f) Sound transmission loss (STL) spectra for the flat and curved meta-curtains.

2.2. Band Structure and Eigenstate Analysis

To obtain the acoustic performance of the meta-curtain, full-wave simulations are performed by COMSOL Multiphysics [49]. The meshes for all the simulations are free tetrahedral and are enough to obtain convergence results. The material parameters of the background medium air are set as $\rho_0 = 1.21 \text{ kg/m}^3$ (mass density) and $c_0 = 343 \text{ m/s}$ (sound velocity). The material parameters of the PVC films are $\rho_1 = 1400 \text{ kg/m}^3$ (mass density), $E_1 = 3 \text{ Gpa}$ (Young's modulus) and $\nu_1 = 0.4$ (Poisson's ratio). Different from the rigid structures used in the previous literatures, the acoustic-structure interactions should be taken into consideration in our design. Figure 1c shows the band structure of a flat meta-curtain (i.e., $\bar{K} = 0$). The geometrical parameters are $D = 5 \text{ cm}$, $l = 20 \text{ cm}$, $h = 1 \text{ cm}$, $t = 0.8 \text{ mm}$ and $\alpha = 0^\circ$, respectively. The open ratio is about 5%, which is defined as $\pi D^2/4l^2$. Here, periodic conditions are employed in COMSOL. It is clearly seen that one resonance appears at 1043 Hz (marked by a red star) and the band gap emerges. The eigenstate of such resonance is plotted in the first inset in Figure 1d. The band gaps are usually used to attenuate sound waves [19].

Interestingly, the symmetry of the eigenstates plays an important role in eventually realizing a large bandwidth for soundproofing. There are three branches (two are degenerate) above the first pass band. We investigate these eigenstates at the Z point marked by orange stars in Figure 1c. As shown in Figure 1d, the eigenstates at 1220 Hz and 1458 Hz are found to be antisymmetric in the xy plane. Such antisymmetric modes are well known as the deaf bands [50], which cannot be excited by incident waves along ΓZ direction. Therefore, the effective band gap for soundproofing is significantly enlarged, which covers the regime from 1043 Hz to 1700 Hz, as marked by grey area in Figure 1c. Such a large band gap indicates the broadband soundproofing property. It is noted that the wavelength at 1043 Hz ($\sim 33 \text{ cm}$) is nearly 28.3 times of the total thickness of the meta-unit (1.16 cm), which confirms the sub-wavelength geometry of the meta-curtain.

2.3. Sound Transmission Loss Analysis

We calculate the sound transmission loss (STL) of the flat meta-curtain, as shown in blue symbol lines in Figure 1e. Here, a plane wave radiation is employed in COMSOL. The dissipation effect is considered by the narrow-region model in the simulations. It is clearly observed that the STL value increases sharply from 1050 Hz and approaches a peak of 51 dB at 1350 Hz, and then gradually decreases to a dip at 1720 Hz. Such soundproofing frequency regime (marked by grey area in Figure 1f) is well matched with the band gap in Figure 1c, further demonstrating the broadband soundproofing functionality.

Moreover, a curved case is investigated. The rotation angle of the tangent is chosen as $\alpha = \pi/3$ and the other geometric parameters are unchanged. Then, the averaged curvature for the curved unit cell is calculated as $\bar{K} = 5.2$. The corresponding eigenstates and the STL spectrum are shown in Figure 1e and as the olive symbol lines in Figure 1f, respectively. Similar to the flat one, the broadband soundproofing functionality for the curved meta-curtain is clearly demonstrated, except for a tiny frequency shift, which could be attributed to the acoustic-structure coupling under the deformation.

3. Fabrication and Experimental Measurement of Flexible Meta-Curtain

3.1. Fabricated Unit Cell and Measurement of Sound Transmission Loss

Then, we fabricate a real unit cell of the meta-curtain, namely meta-unit, as shown in Figure 2a. The meta-unit is made up of two transparent PVC films fixed on a perforated acrylic sheet. The geometrical parameters are $D = 5 \text{ cm}$, $l = 20 \text{ cm}$, $h = 1 \text{ cm}$, $t = 0.8 \text{ mm}$, and $\alpha = 0^\circ$. Then, the meta-unit is closely sandwiched between two parts of the acoustic waveguide formed by PMMA (polymethyl methacrylate) plates with a cross-section of $20 \text{ cm} \times 20 \text{ cm}$, as shown in Figure 2b. The corresponding diagram of the experimental setup is also shown in Figure 2c. One sound speaker (HiVi M4N) (used as a source) and one microphone (GRAS46BE) (used as a detector) are placed at the front and back ends of the waveguide, respectively. The speaker and the microphone are both 30 cm away from the

sample. Sound absorbing foams are put around the waveguide to eliminate the influence of unwanted reflection. For comparison, we stack these two films together to form a pure perforated film with a thickness of 1.6 mm. Such a contrast sample has the same weight as the meta-unit, but there is no acoustic cavity inside.

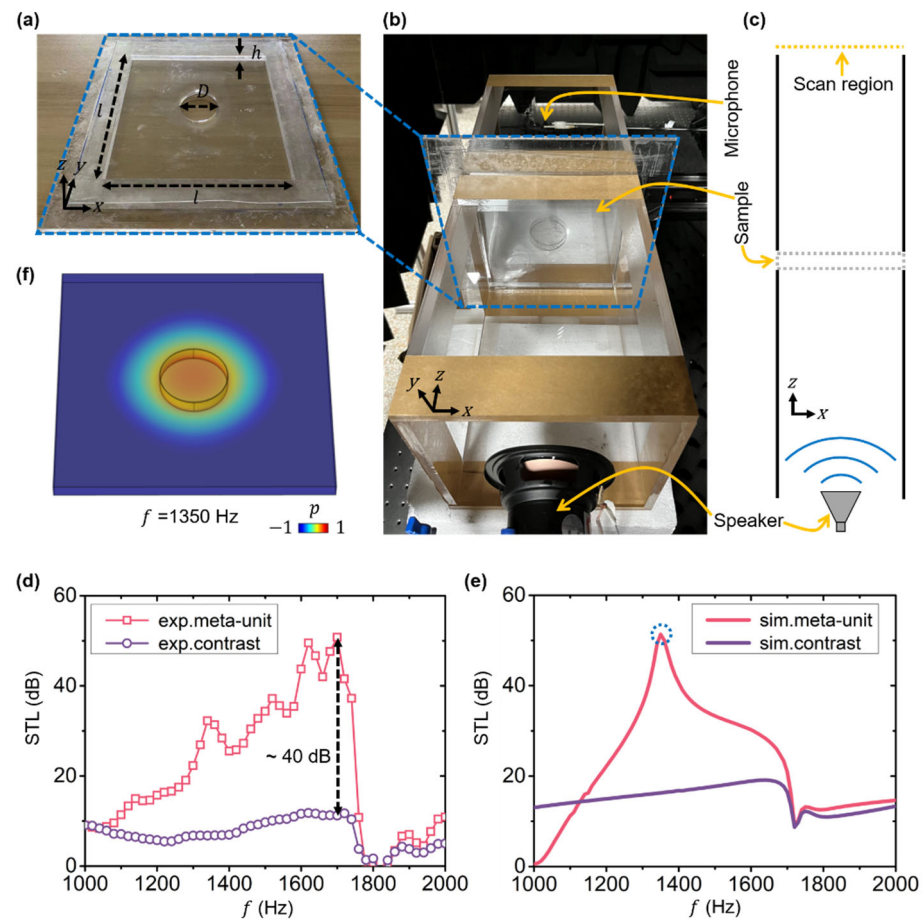


Figure 2. (a) Photograph of a meta-unit of the meta-curtain. (b) Photograph and (c) diagram of the experimental platform of the one-dimensional acoustic waveguide. (d) Measured and (e) simulated STL spectra for the meta-unit and the contrast. (f) Simulated acoustic pressure field distribution for the meta-unit located at the STL peak of 1350 Hz.

The measured results for the meta-unit and the contrast sample are plotted in Figure 2d. The STL is a normalized quantity defined as $-20 \log |p_1/p_0|$, where p_1 and p_0 denote the sound pressure (measured in Pa) with and without the sample, respectively. For the contrast sample, the STL profile is flat in the spectral range from 1000 Hz to 2000 Hz, and the value is relatively lower (~ 10 dB). While the STL value for the meta-unit is larger than that of the contrast within a large bandwidth approximately from 1040 Hz to 1750 Hz. The STL difference between the meta-unit and the contrast approaches the maximum of 40 dB near 1700 Hz. We note that the wavelength at 1700 Hz is about 20 cm, which is nearly 17.4 times of the total thickness of the meta-unit (1.16 cm). As plotted in Figure 2e, the similar soundproofing performance is clearly observed in the simulations, where the bandwidth of enhanced soundproofing is from 1100 Hz to 1700 Hz, which is approximately the same range as the experimental results. The resonance at 1350 Hz induced by the acoustic cavity is plotted in Figure 2f. The STL profiles in experiments and simulations are consistent with each other. The discrepancy between the experimental and simulation results could be a result of the fabrication tolerance and the inaccurate material parameters in practice. The additional minor fluctuations in the measured results could be attributed to the structural vibrations of the soft PVC films.

3.2. Fabricated Full-Size Meta-Curtain and Measurement of Sound Transmission Loss

Further, we fabricate a full-size meta-curtain to verify the soundproofing properties in a larger scale. The photograph and diagram of the meta-curtain and the experimental setup are shown in Figure 3a,b. The meta-curtain is constructed with nine unit-cells in 3×3 square lattice. The geometry of the unit cell is the same as that in Figure 2. Sixteen tiny pillars (with a diameter of 5 mm and a height of 1 cm) are fixed between two films to guarantee the distance of 1 cm. The frame of the meta-curtain is fabricated with soft rubber strips with a height of 1 cm and a width of 5 mm. The whole size of the meta-curtain is 61 cm \times 61 cm with a thickness of 1.16 cm. The total weight is 0.72 kg. Such a meta-curtain is pasted to cover a square open hole of polypropylene board, which can be considered as an open window. The size of the open hole on the hard board is 50 cm \times 50 cm. One sound speaker (the source) and one microphone (the detector) are put on the front and back sides of the board, respectively. The speaker is placed 1 m away from the meta-curtain and oriented toward it. The microphone to measure the acoustic signals is mounted on the stage at 30 cm away from the meta-curtain. Sound-absorbing foams are placed around the whole system to prevent the leaky waves and reduce the reflection. For comparison, a similar contrast sample (a pure open-hole film with a thickness of 1.6 mm) is also investigated.

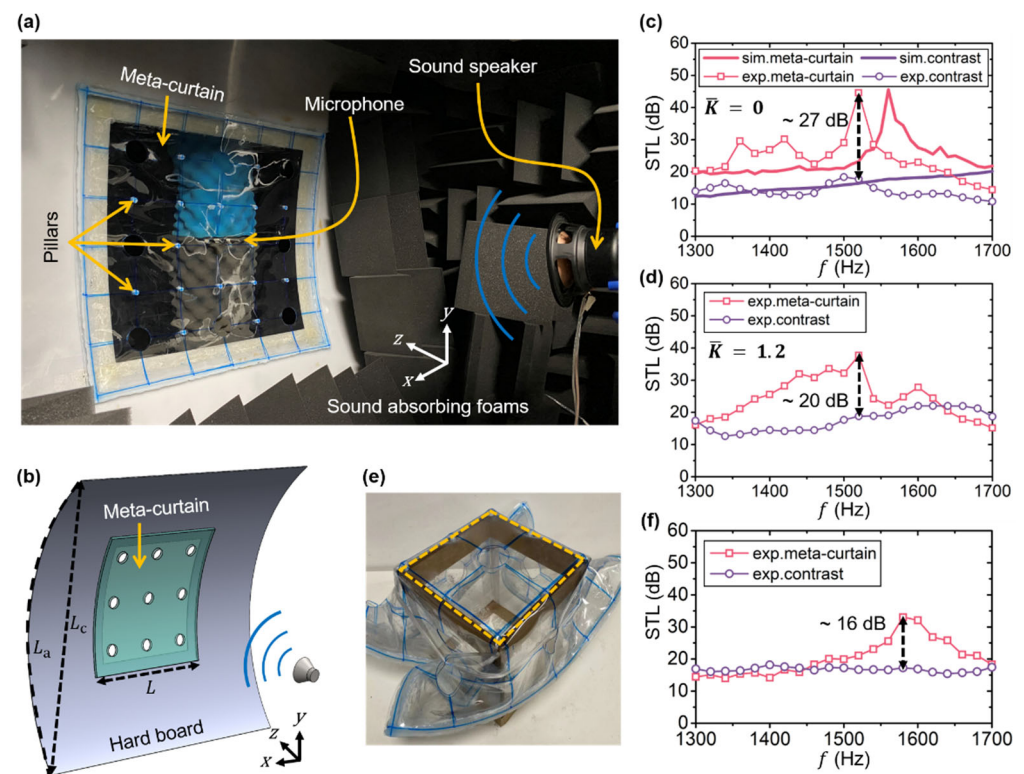


Figure 3. (a) Photograph and (b) diagram of the three-dimensional experimental setup. (c) Measured and simulated STL spectra for a flat meta-curtain with $\bar{K} = 0$. (d) Measured STL spectra for a curved meta-curtain with $\bar{K} = 1.2$. (e) Photograph of a square-shaped pipe tightly sealed by the flexible meta-curtain. (f) Measured STL spectra for the case of (e).

In order to demonstrate the flexibility of the meta-curtain, we consider bending the polypropylene board, and the attached meta-curtain is deformed accordingly. The averaged curvature can be obtained by measuring the arc length L_a and the chord length L_c , as schematically shown in Figure 3b. In the first case, we consider a flat case of $\bar{K} = 0$. The STL profiles are obtained in both experiments and simulations and plotted in Figure 3c. Here, a point source radiation is employed in simulations. The simulated results are well consistent with the experimental results. From the measured results, it is seen that the STL value of the flat meta-curtain is generally larger than that of the contrast sample over the

frequency range from 1300 Hz to 1700 Hz and has a peak of 45 dB at 1520 Hz. The maximal STL difference between the meta-curtain and the contrast sample is 27 dB at 1520 Hz. We note that the peak position moves from 1700 Hz to 1520 Hz in comparison with the result shown in Figure 2d, which could be attributed to the diffraction coupling effect of the periodic structure.

In the second case, a curved meta-curtain is considered. We find the arc length is $L_a = 1.2$ m and the chord length is $L_c = 1.1$ m. If we assume the arc is a part of a circle, then the rotation angle of the tangent can be obtained as $\alpha = 1.43$ and the averaged curvature is $\bar{K} = 1.2$. Figure 3d shows the measured STL spectra for $\bar{K} = 0$. It is seen that the curved meta-curtain can still maintain a good soundproofing performance in a wide frequency ranging from 1300 Hz to 1620 Hz. The position of the STL peak is still at 1520 Hz, which drops slightly to 38 dB. The difference in the STL spectra of the meta-curtain for the two cases of $\bar{K} = 0$ and $\bar{K} = 1.2$ stems from the structural deformation.

To further exhibit the advantages of flexibility and deformability, in the third case, we tie the meta-curtain tightly around the opening of a pipe with string, as shown in Figure 3e. We consider a similar measuring method as discussed above. Sound wave is emitted by a speaker outside the pipe and a microphone is placed inside the pipe to detect the signal. The soundproofing performance is verified through measuring the transmitted signal. The speaker or microphone is 60 cm or 30 cm away from the meta-curtain, respectively. Benefiting from the pillars between the films, the cavity structure marked by orange-dotted-line domain is kept relatively intact. Other area of the meta-curtain is fixed tightly to the side wall of pipe such that there is almost no leaky energy. The measured results plotted in Figure 3f indicate broadband soundproofing functionality. An STL peak of 33 dB appears at 1580 Hz for the meta-curtain, and the maximal STL difference between the meta-curtain and the contrast is 16 dB at 1580 Hz. The bandwidth of enhanced soundproofing is from 1450 Hz to 1700 Hz. We note that the elastic tension of the films could reduce the distance between the films at some places, which could be responsible for the frequency shift in comparison with the results in Figure 3c,d.

4. Tunability on Geometrical Parameters

Finally, we systematically study the influence of the geometrical parameters of the meta-curtain and demonstrate its tunability. Here, we consider a single flat meta-unit model illustrated in Figure 2 and calculate the STL spectra. In Figure 4a, the STL spectra as a function of the film thickness is plotted with $h = 1$ cm, $D = 5$ cm and $l = 20$ cm. It is seen that the STL peak is shifted to a higher frequency when t decreases. When t decreases to 0.5 mm, the STL peak dramatically drops to 30 dB and the bandwidth shrinks. This indicates that there is a limit of the minimum film thickness for soundproofing. When t increases to a certain value, the frequency range of soundproofing converges to a regime determined by the resonance in the acoustic cavity. In Figure 4b, the STL spectra as a function of the cavity height is plotted with $t = 0.8$ mm, $D = 5$ cm and $l = 20$ cm. When h decreases to 0.5 cm, the STL peak also dramatically drops to 30 dB and the bandwidth shrinks. This indicates that there is also a limit of the minimum cavity height in the formation of the resonance for soundproofing. When h increases to be larger than 2 cm, the STL peak and bandwidth becomes almost independent of h . Figure 4c shows the STL spectra as a function of the central-hole diameter, as plotted with $t = 0.8$ mm, $h = 1$ cm and $l = 20$ cm. It turns out that the frequency of the STL peak is relatively insensitive to D , while the performance and bandwidth of STL decrease as D increases. This indicates a trade-off between the performances of soundproofing and ventilation. Figure 4d shows the STL spectra as a function of the lattice constant, as plotted with $t = 0.8$ mm, $h = 1$ cm and $D = 5$ cm. The results indicate that meta-unit of a larger size has a lower resonance frequency. Overall, the meta-curtain exhibits rich parameters and a strong ability to tailor the soundproofing performance.

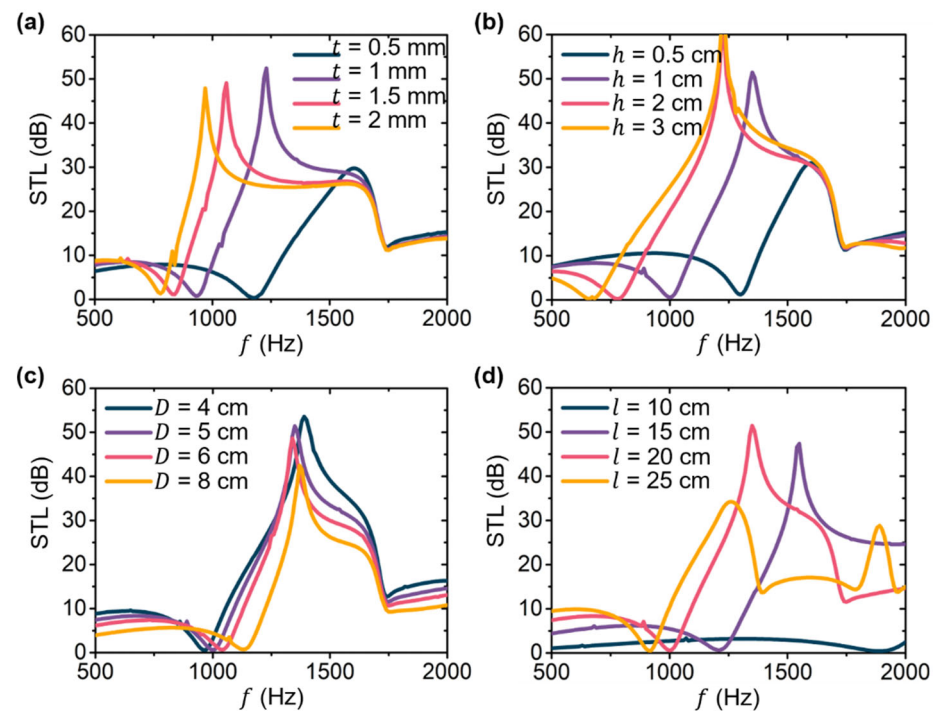


Figure 4. Simulated STL spectra as a function of (a) the thickness of the film, (b) the height of the air cavity, (c) the diameter of the central hole, and (d) the lattice constant of the meta-unit.

5. Conclusions

In summary, our work has demonstrated a flexible meta-curtain for soundproofing and ventilation, based on soft and flexible materials such as perforated PVC films and tiny pillars. A large band gap for soundproofing is observed in the low frequency regime of the band structure, which is an interesting consequence of the asymmetric modes therein as deaf bands. Large STL over a broad bandwidth is verified in both simulations and experiments, which is bestowed by the resonances formed between the films. The total thickness is 1.16 cm, and the weight is 0.72 kg for the designed meta-curtain. Open holes with a diameter of 5 cm enable good ventilation, which could meet the demands of heat dissipation and fresh air. The potential applications include working rooms that need sound insulation and fresh air, and machine rooms that seek the techniques of sound insulation and heat dissipation. A significant advantage of this meta-curtain is that it could retain its soundproofing and ventilation properties even under deformation. Our design has the attractive features of flexibility, sub-wavelength thickness, and easy fabrication, which suggest that it could have practical applications for noise control.

Author Contributions: X.C., C.L. and J.S. contributed equally to this work. C.S. helped sample fabrication. X.L. and Y.L. provided guidance. All authors have read and agreed to the published version of the manuscript.

Funding: This work is supported by the National Key R&D Program of China (Grant No. 2020YFA0211400) and the National Natural Science Foundation of China (Grants No. 11974176, No. 12174188, No. 12174192 and No. 12174193).

Institutional Review Board Statement: Not applicable.

Informed Consent Statement: Not applicable.

Data Availability Statement: The data that support the findings of this study are available within this article.

Conflicts of Interest: The authors have no conflict to disclose.

References

1. Kang, J.; Brocklesby, M.W. Feasibility of applying micro-perforated absorbers in acoustic window systems. *Appl. Acoust.* **2005**, *66*, 669–689. [[CrossRef](#)]
2. Ma, G.; Sheng, P. Acoustic metamaterials: From local resonances to broad horizons. *Sci. Adv.* **2016**, *2*, e1501595. [[CrossRef](#)] [[PubMed](#)]
3. Assouar, B.; Liang, B.; Wu, Y.; Li, Y.; Cheng, J.C.; Jing, Y. Acoustic metasurfaces. *Nat. Rev. Mater.* **2018**, *3*, 460–472. [[CrossRef](#)]
4. Zhang, S.; Xia, C.; Fang, N. Broadband acoustic cloak for ultrasound waves. *Phys. Rev. Lett.* **2011**, *106*, 024301. [[CrossRef](#)]
5. Sanchis, L.; García-Chocano, V.M.; Llopis-Pontiveros, R.; Climente, A.; Martínez-Pastor, J.; Cervera, F.; Sánchez-Dehesa, J. Three-dimensional axisymmetric cloak based on the cancellation of acoustic scattering from a sphere. *Phys. Rev. Lett.* **2013**, *110*, 124301. [[CrossRef](#)]
6. Zigoneanu, L.; Popa, B.I.; Cummer, S.A. Three-dimensional broadband omnidirectional acoustic ground cloak. *Nat. Mater.* **2014**, *13*, 352–355. [[CrossRef](#)]
7. Zhang, X.; Xiao, M.; Cheng, Y.; Lu, M.H.; Christensen, J. Topological sound. *Commun. Phys.* **2018**, *1*, 97. [[CrossRef](#)]
8. Ma, G.; Xiao, M.; Chan, C.T. Topological phases in acoustic and mechanical systems. *Nat. Rev. Phys.* **2019**, *1*, 281–294. [[CrossRef](#)]
9. Xue, H.; Yang, Y.; Zhang, B. Topological acoustics. *Nat. Rev. Mater.* **2022**, *1*, 17. [[CrossRef](#)]
10. Qu, S.; Gao, N.; Tinel, A.; Morvan, B.; Groby, P.; Sheng, P.; Bay, W.; Kong, H. Underwater metamaterial absorber with impedance-matched composite. *Sci. Adv.* **2022**, *8*, eabm4206. [[CrossRef](#)]
11. Kim, S.H.; Lee, S.H. Air transparent soundproof window. *AIP Adv.* **2014**, *4*, 117123. [[CrossRef](#)]
12. Kurdi, M.H.; Duncan, G.S.; Nudahi, S.S. Optimal design of a helmholtz resonator with a flexible end plate. *J. Vib. Acoust.* **2014**, *136*, 031004. [[CrossRef](#)]
13. Cheng, Y.; Zhou, C.; Yuan, B.G.; Wu, D.J.; Wei, Q.; Liu, X.J. Ultra-sparse metasurface for high reflection of low-frequency sound based on artificial Mie resonances. *Nat. Mater.* **2015**, *14*, 1013–1019. [[CrossRef](#)] [[PubMed](#)]
14. Jiménez, N.; Romero-García, V.; Pagneux, V.; Groby, J.P. Quasiperfect absorption by subwavelength acoustic panels in transmission using accumulation of resonances due to slow sound. *Phys. Rev. B* **2017**, *95*, 014205. [[CrossRef](#)]
15. Jung, J.W.; Kim, J.E.; Lee, J.W. Acoustic metamaterial panel for both fluid passage and broadband soundproofing in the audible frequency range. *Appl. Phys. Lett.* **2018**, *112*, 041903. [[CrossRef](#)]
16. Wu, X.; Au-Yeung, K.Y.; Li, X.; Roberts, R.C.; Tian, J.; Hu, C.; Huang, Y.; Wang, S.; Yang, Z.; Wen, W. High-efficiency ventilated metamaterial absorber at low frequency. *Appl. Phys. Lett.* **2018**, *112*, 103505. [[CrossRef](#)]
17. Yang, J.; Lee, J.S.; Lee, H.R.; Kang, Y.J.; Kim, Y.Y. Slow-wave metamaterial open panels for efficient reduction of low-frequency sound transmission. *Appl. Phys. Lett.* **2018**, *112*, 091901. [[CrossRef](#)]
18. Li, L.J.; Zheng, B.; Zhong, L.M.; Yang, J.; Liang, B.; Cheng, J.C. Broadband compact acoustic absorber with high-efficiency ventilation performance. *Appl. Phys. Lett.* **2018**, *113*, 103501. [[CrossRef](#)]
19. Lee, T.; Nomura, T.; Dede, E.M.; Iizuka, H. Ultrasparse Acoustic Absorbers Enabling Fluid Flow and Visible-Light Controls. *Phys. Rev. Appl.* **2019**, *11*, 024022. [[CrossRef](#)]
20. Lee, T.; Nomura, T.; Iizuka, H. Damped resonance for broadband acoustic absorption in one-port and two-port systems. *Sci. Rep.* **2019**, *9*, 13077. [[CrossRef](#)]
21. Su, X.; Banerjee, D. Extraordinary sound isolation using an ultrasparse array of degenerate anisotropic scatterers. *Phys. Rev. Appl.* **2020**, *13*, 064047. [[CrossRef](#)]
22. Kim, D.-Y.; Ih, J.-G. Wideband reduction of in-duct noise using acoustic metamaterial with serially connected resonators made. *Appl. Phys. Lett.* **2020**, *116*, 251904. [[CrossRef](#)]
23. Nguyen, H.; Wu, Q.; Xu, X.; Chen, H.; Tracy, S.; Huang, G. Broadband acoustic silencer with ventilation based on slit-type Helmholtz resonators. *Appl. Phys. Lett.* **2020**, *117*, 134103. [[CrossRef](#)]
24. Kumar, S.; Xiang, T.B.; Lee, H.P. Ventilated acoustic metamaterial window panels for simultaneous noise shielding and air circulation. *Appl. Acoust.* **2020**, *159*, 107088. [[CrossRef](#)]
25. Melnikov, A.; Maeder, M.; Friedrich, N.; Pozhanka, Y.; Wollmann, A.; Scheffler, M.; Oberst, S.; Powell, D.; Marburg, S. Acoustic metamaterial capsule for reduction of stage machinery noise. *J. Acoust. Soc. Am.* **2020**, *147*, 1491–1503. [[CrossRef](#)] [[PubMed](#)]
26. Dong, R.; Mao, D.; Wang, X.; Li, Y. Ultrabroadband Acoustic Ventilation Barriers via Hybrid-Functional Metasurfaces. *Phys. Rev. Appl.* **2021**, *15*, 024044. [[CrossRef](#)]
27. Liu, C.; Shi, J.; Zhao, W.; Zhou, X.; Ma, C.; Peng, R.; Wang, M.; Hang, Z.H.; Liu, X.; Christensen, J.; et al. Three-Dimensional Soundproof Acoustic Metacage. *Phys. Rev. Lett.* **2021**, *127*, 084301. [[CrossRef](#)]
28. Fusaro, G.; Yu, X.; Lu, Z.; Cui, F.; Kang, J. A metawindow with optimised acoustic and ventilation performance. *Appl. Sci.* **2021**, *11*, 3168. [[CrossRef](#)]
29. Shen, L.; Zhu, Y.; Mao, F.; Gao, S.; Su, Z.; Luo, Z.; Zhang, H.; Assouar, B. Broadband Low-Frequency Acoustic Metamuffler. *Phys. Rev. Appl.* **2021**, *16*, 064057. [[CrossRef](#)]
30. Xiang, X.; Tian, H.; Huang, Y.; Wu, X.; Wen, W. Manually tunable ventilated metamaterial absorbers. *Appl. Phys. Lett.* **2021**, *118*, 053504. [[CrossRef](#)]
31. Liu, C.; Wang, H.; Liang, B.; Cheng, J.; Lai, Y. Low-frequency and broadband muffler via cascaded labyrinthine metasurfaces. *Appl. Phys. Lett.* **2022**, *120*, 231702. [[CrossRef](#)]

32. Ma, G.; Yang, M.; Yang, Z.; Sheng, P. Low-frequency narrow-band acoustic filter with large orifice. *Appl. Phys. Lett.* **2013**, *103*, 011903. [[CrossRef](#)]
33. Zhang, H.L.; Zhu, Y.F.; Liang, B.; Yang, J.; Yang, J.; Cheng, J.C. Omnidirectional ventilated acoustic barrier. *Appl. Phys. Lett.* **2017**, *111*, 203502. [[CrossRef](#)]
34. Wang, X.; Luo, X.; Yang, B.; Huang, Z. Ultrathin and durable open metamaterials for simultaneous ventilation and sound reduction. *Appl. Phys. Lett.* **2019**, *115*, 171902. [[CrossRef](#)]
35. Ghaffarivardavagh, R.; Nikolajczyk, J.; Anderson, S.; Zhang, X. Ultra-open acoustic metamaterial silencer based on Fano-like interference. *Phys. Rev. B* **2019**, *99*, 024302. [[CrossRef](#)]
36. Sun, M.; Fang, X.; Mao, D.; Wang, X.; Li, Y. Broadband Acoustic Ventilation Barriers. *Phys. Rev. Appl.* **2020**, *13*, 044028. [[CrossRef](#)]
37. Shi, J.; Liu, C.; Liu, X.; Lai, Y. Ventilative meta-window with broadband low-frequency acoustic insulation. *J. Appl. Phys.* **2021**, *129*, 094901. [[CrossRef](#)]
38. Nguyen, H.Q.; Wu, Q.; Chen, H.; Chen, J.J.; Yu, Y.K.; Tracy, S.; Huang, G.L. A Fano-based acoustic metamaterial for ultra-broadband sound barriers. *Proc. R. Soc. A* **2021**, *477*, 20210024. [[CrossRef](#)]
39. Xu, Z.X.; Zheng, B.; Yang, J.; Liang, B.; Cheng, J.C. Machine-Learning-Assisted Acoustic Consecutive Fano Resonances: Application to a Tunable Broadband Low-Frequency Metasilencer. *Phys. Rev. Appl.* **2021**, *16*, 044020. [[CrossRef](#)]
40. García-Chocano, V.M.; Cabrera, S.; Sánchez-Dehesa, J. Broadband sound absorption by lattices of microperforated cylindrical shells. *Appl. Phys. Lett.* **2012**, *101*, 184101. [[CrossRef](#)]
41. Xu, Z.; Gao, H.; Ding, Y.; Yang, J.; Liang, B.; Cheng, J. Topology-Optimized Omnidirectional Broadband Acoustic Ventilation Barrier. *Phys. Rev. Appl.* **2020**, *10*, 054016. [[CrossRef](#)]
42. Zhang, H.L.; Zhu, Y.F.; Liang, B.; Yang, J.; Yang, J.; Cheng, J.C. Sound Insulation in a Hollow Pipe with Subwavelength Thickness. *Sci. Rep.* **2017**, *7*, 44106. [[CrossRef](#)] [[PubMed](#)]
43. Shen, C.; Xie, Y.; Li, J.; Cummer, S.A.; Jing, Y. Acoustic metacages for sound shielding with steady air flow. *J. Appl. Phys.* **2018**, *123*, 124501. [[CrossRef](#)]
44. Ge, Y.; Sun, H.X.; Yuan, S.Q.; Lai, Y. Switchable omnidirectional acoustic insulation through open window structures with ultrathin metasurfaces. *Phys. Rev. Mater.* **2019**, *3*, 065203. [[CrossRef](#)]
45. Kumar, S.; Lee, H.P. Recent advances in acoustic metamaterials for simultaneous sound attenuation and air ventilation performances. *Crystals* **2020**, *10*, 686. [[CrossRef](#)]
46. Dong, R.; Sun, M.; Mo, F.; Mao, D.; Wang, X.; Li, Y. Recent advances in acoustic ventilation barriers. *J. Phys. D: Appl. Phys.* **2021**, *54*, 403002. [[CrossRef](#)]
47. Lee, H.P.; Kumar, S. Perspectives on the Sonic Environment and Noise Mitigations during the COVID-19 Pandemic Era. *Acoustics* **2021**, *3*, 493–506. [[CrossRef](#)]
48. Fang, N.; Xi, D.; Xu, J.; Ambati, M.; Srituravanich, W.; Sun, C.; Zhang, X. Ultrasonic metamaterials with negative modulus. *Nat. Mater.* **2006**, *5*, 452–456. [[CrossRef](#)]
49. Roger, W. *Pryor Multiphysics Modeling Using COMSOL: A First Principles Approach*; Jones & Bartlett Learning: Sudbury, MA, Canada, 2011.
50. Indaleeb, M.M.; Banerjee, S.; Ahmed, H.; Saadatzi, M.; Ahmed, R. Deaf band based engineered Dirac cone in a periodic acoustic metamaterial: A numerical and experimental study. *Phys. Rev. B* **2019**, *99*, 024311. [[CrossRef](#)]